Available online at www.sciencedirect.com
ScienceDirect
Cement and Concrete Research 37 (2007) 1598–1612
Cement and Concrete Research

Influence of impressed current on the initiation of damage in reinforced mortar due to corrosion of embedded steel

Sabine Caré [a,*], André Raharinaivo [b]

[a] Université Paris-Est, Institut Navier, LMSGC (LCPC / ENPC / CNRS), 2, allée Kepler, 77420 Champs sur Marne, France
[b] Laboratoire Central des Ponts et Chaussées, 58 Bd Lefebvre, 75732 Paris, France

Received 11 July 2005; accepted 25 August 2007

Abstract

Corrosion of steel in cementitious material is a slow process. Therefore in this study, accelerated corrosion tests were carried out by impressing current between steel embedded in mortar and a counter-electrode to study the process of corrosion leading to cracking in mortar. The specimens, which were made of mortar reinforced with steel, were immersed in solutions which contained or did not contain chlorides.

Critical times with respect to the onset of corrosion can be defined in various ways by using either steel half-cell potential, or potential drop between embedded steel and a counter-electrode, or expansion of the mortar specimen. These parameters give quite similar critical times and are related to the development of corrosion products and microcracking. The results obtained provide information on corrosion kinetics of embedded steel when corrosion is accelerated by impressed current and show the similarities to natural corrosion pattern when solutions contain chlorides.

Keywords: Microcracking; Accelerated reinforcement corrosion; Electrochemical properties; Expansion; Mortar

1. Introduction and objective

The service lifetime of a reinforced concrete structure can be reduced by corrosion of the embedded reinforcing steel. Such corrosion is due to aggressive agents which come from the ambient environment. The most harmful aggressive agent is chloride contained either in seawater or in deicing salts. Under chloride attack, the passive film is locally damaged and steel starts to dissolve in these unprotected areas. Thereupon, depassivated areas grow and the amount of corrosion products increases. When these products are solid, their volume is higher than that of the original metal. As this volume gradually increases, a pressure is induced around the embedded steel, and the concrete cover expands up to possible cracking, spalling or delamination [1].

Different conceptual models are proposed to describe the corrosion process of steel in concrete [2–4]. According to [2], under natural conditions, steel corrosion in concrete includes two consecutive stages which include “initiation”, when aggressive agents enter concrete without depassivating steel, and “propagation”, when corrosion is initiated, so that rust forms and expands around the steel and induces cover swelling or cracking. According to [3], three consecutive distinct stages are to be considered involving diffusion of aggressive agents, steel corrosion and cover deterioration. The first stage is the same as the initiation stage described by [2]. The second stage corresponds to the development of corrosion products resulting in the first damage and the third stage (deterioration) starts when the damaged reinforced concrete structure needs to be rehabilitated. These models for steel corrosion in concrete were complemented in [4], which takes into account the initial micro-cracks in the concrete cover, which can modify the initiation period.

In fact, under natural conditions the process of reinforcement corrosion is very slow; usually the first crack observed on the outer concrete surface appears after many years. So laboratory studies need an acceleration of corrosion process to achieve a short test period. This can be accomplished by applying a constant potential [5,6] or an electric current of constant magnitude [7–9] to the embedded steel. In accelerated tests,

* Corresponding author. LMSGC, 2, allée Kepler, 77420 Champs sur Marne, France.
E-mail address: care@lcpc.fr (S. Caré).

0008-8846/$ - see front matter © 2007 Elsevier Ltd. All rights reserved.
doi:10.1016/j.cemconres.2007.08.022

Table 1
Mortar designs

Mortar	Weight (g)	
	Mortar M1	Mortar M2
Water	225	288
Cement	450	618
Siliceous sand 0/2 mm	1350	/
Siliceous–calcareous sand 0/4 mm	/	1350
Water-cement ratio (W/C)	0.50	0.46

chloride penetration is enhanced by ion migration; corrosion rate is increased by an electric field on steel surface. The results obtained have several applications. Accelerated corrosion tests are carried out by [6,7] to understand the effect of corrosion on bond strength of reinforced concrete. Cracking of the cover versus rebar corrosion is studied in [8,9].

Thus, this method appears as an interesting procedure to evaluate the effect of reinforcement corrosion on concrete damage because it allows reducing the test period. But this method possibly modifies the corrosion process and the corrosion pattern due to iron migration in concrete pores. The objective of this study is to check how an impressed current can be used to shorten the corrosion critical times leading to mortar swelling and cracking. To determine corrosion kinetics induced by impressed technique, it is proposed to use mechanical measurements (expansion) and electrochemical parameters (potential drop and half-cell potential). It is to be noted that rust expansion around reinforcement can result in concrete cover expansion and cracking, as well as loss of bonding between steel and concrete. The accelerated process of steel corrosion and cover swelling under accelerated tests is compared to the similar process under natural conditions. This comparison concerns also the corrosion pattern obtained. To validate this method for evaluating the effect of corrosion on mortar damage, it is important to verify that corrosion products are formed at the interface between steel and mortar and may induce pressure around the embedded steel. Previous published results have given no data on corrosion pattern when high current density is used to accelerate the corrosion process. So, this study is focused on characterizing the effect of an accelerated corrosion of rebar on the resulting change of steel–concrete interface.

2. Experimental program

2.1. Specimen

The designs of the two mortars (labeled M1 and M2), are presented in Table 1: mortar M1 is a standard mix used by several authors [5] and mortar M2 is used in industrial application [10]. The cement was an ordinary Portland Cement (European grade CEM I, 52.5); its chemical analysis is given in Table 2. The aggregate in mortar M1 was a siliceous sand (0/2 mm, standard sand ISO 679), and in mortar M2 it was a siliceous–calcareous sand (0/4 mm).

Table 2
Components of Portland cement

C3S	C2S	C3A	C4AF
61.9%	15.4%	8.8%	9.1%

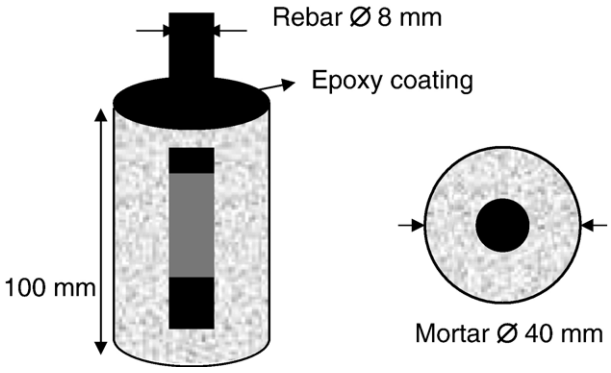

Fig. 1. Test specimen.

The reinforcement was a plain carbon steel wire, 8 mm in diameter and 100 mm long. After being polished with abrasive papers and rinsed with distilled water, the steel surface was coated with an electric insulator, except for a zone, with an area of 12.5 cm^2 for mortar M1 and 21 cm^2 for mortar M2. This uncoated area was to be embedded in mortar.

After mixing, the fresh mortar was poured into a cylindrical plastic mould (40 mm in diameter and 100 mm high) where the reinforcement was previously placed along its longitudinal axis (Fig. 1). So, the cover thickness of the specimens amounted to 16 mm. The specimen was then compacted during 60 s by using a vibrating table. The specimens were stored at room temperature, in 100% relative humidity (RH) during at least three months before testing. Thus, their microstructure did not change significantly during the experimentations. The microstructure features of mortars M1 and M2 were characterized by scanning electron microscopy (SEM) and by mercury intrusion porosimetry (MIP).

2.2. Accelerated corrosion tests

The accelerated corrosion tests deal with placing reinforced mortar specimen in a solution, and polarizing the

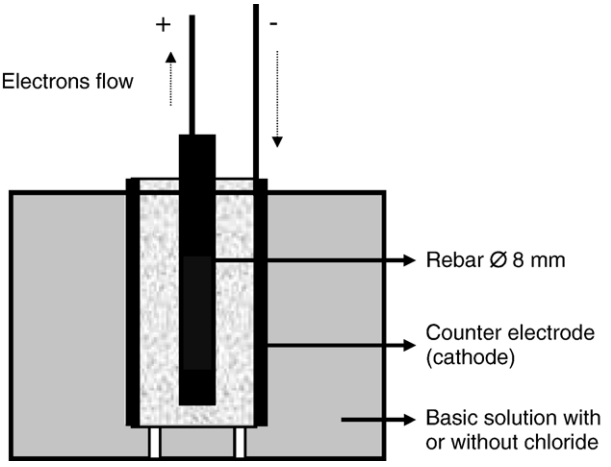

Fig. 2. Scheme of the experimental set-up.

Table 3
Experimental program

	Mortar M1				Mortar M2		
	$j=100$ μA/cm^2		$j=500$ μA/cm^2		$j=100$ μA/cm^2	$j=500$ μA/cm^2	
Solution	A	B	A	B	A	A	B
Number of tests	3	3	1	3	1	1	2
Duration of corrosion (days)	24	34	13	13	24	24	13

Solution A: alkaline solution with 1 g/l NaOH+4.65 g/l KOH.
Solution B: alkaline solution with 1 g/l NaOH+4.65 g/l KOH with [Cl^-]=18 g/L.

reinforcement anodically against a counter-electrode to enhance its corrosion.

The specimens were immersed in two types of solutions:

- an alkaline solution with 1 g/L NaOH+4.65 g/L KOH in water and
- the same solution with 30 g/L NaCl (so, [Cl^-]=18 g/L).

A power supply was used for applying a constant, direct current between reinforcement and a counter-electrode, made of carbon fiber mesh. This counter-electrode was placed around the reinforced mortar specimen in the solution. Fig. 2 shows schematically the experimental set-up. The rebar was connected to the positive pole of the power supply, and thus became anodic. The counter-electrode was connected to the negative pole. A resistor was placed in the external electric circuit to check the magnitude of the current flowing in the system.

The reinforcing steel was polarized by a constant current. The experimental program is shown in Table 3. Two levels of current density j were applied. The lowest level, $j=100$ μA/cm^2, was used by several authors [8]; it corresponds to the highest corrosion rates recorded in existing reinforced concrete structures. The second value $j=500$ μA/cm^2 was chosen to significantly accelerate the corrosion processes.

2.3. Expansion and cracking of specimen

The specimen expansion U (in μm) was measured by using a micrometer. The transverse expansion value was the mean value of several measurements and it is defined by: $U=(D-D_o)/2$, where D_o is the initial diameter of the specimen and D is the specimen diameter during the test. Three measurements were made along the longitudinal axis and on two diameters of each specimen for determining expansion. The measurement accuracy of the expansion U is about ±5 μm. After mortar cracking, U is no more homogeneous as it now characterizes the crack width.

2.4. Electrochemical measurements

The electrochemical parameters, which were measured were potential drop V and half-cell potential E:

- during the corrosion test the potential drop V is measured between the embedded reinforcement bar and the external counter-electrode. As the current density value was constant, V is proportional to a specific electrical resistance R (in Ω cm^2) of the medium between reinforcing steel and counter-electrode.
- the half-cell potential E of the rebar versus a saturated calomel electrode (SCE) reference electrode was measured regularly. For these measurements, polarization was stopped, and specimens were taken out of the solution, and the readings were made approximately 30 min after the current was switched off.

Furthermore, the conductivity of solution around specimens was measured in order to detect any possible effect of the impressed current.

2.5. Characterization of corrosion pattern

At the end of the test, specimens were broken and the condition of steel and mortar were examined visually. Furthermore, this examination makes it possible to characterize the corrosion pattern. The corrosion products and steel–mortar interface features are determined with Optical Microscopy (OM), Energy Dispersive spectrometry (EDS) coupled to Scanning Electron Microscopy (SEM). First, optical microscopy gives a global overview of the interface between steel and mortar. By using SEM with EDS analyses chemical composition of the corrosion products can be determined.

3. Results and analysis

3.1. Microstructure characterization of mortars M1 and M2

The average ultimate compressive strengths of the two mortars are equal to approximately 64 MPa. The pore structure of these mortars was characterized by mercury intrusion

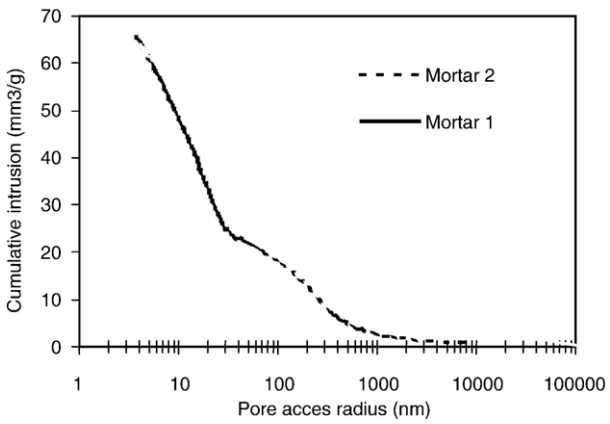

Fig. 3. Cumulative intruded pore volume for the two mortars M1 and M2.

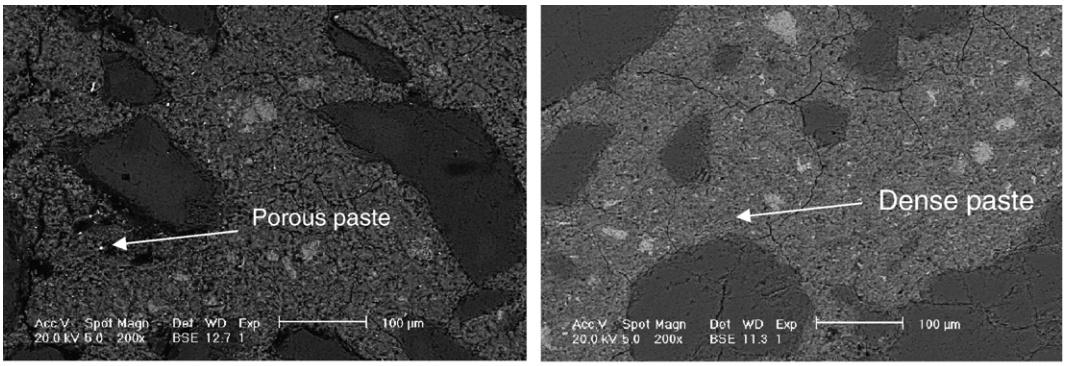

Fig. 4. Scanning electron microscope (SEM) photographs.

porosimetry tests using an apparatus with a maximum of 200 MPa injection pressure and specimen were dried by vacuum-drying technique. With this technique, the total porosity is the ratio between the total injected mercury volume and the total volume of the sample. The total porosity is 13.4% for mortar M1 and 13.8% for mortar M2. Fig. 3 shows that mortar M1 is more porous (more large capillary pores) than mortar M2. These results are confirmed by SEM observations (Fig. 4) where dark gray zones are larger in mortar M1 than in mortar M2. This difference is due to the water-to-cement ratios of mortars, to their aggregate sizes [11] and to the types of sand.

3.2. Expansion and cracking of mortar cover under impressed current

Figs. 5 and 6 give the specimen expansion U in function of time for $j=100$ μA/cm^2 and $j=500$ μA/cm^2. It appears that, for a given time, expansion U strongly depends on the applied current density and on the chloride content in solution. This can be detailed as follows.

When the impressed current density is $j=100$ μA/cm^2:

– For tests with mortar M1: in the absence of chloride, no expansion was detected during accelerated tests, even after 24 days. In the presence of chloride a slight expansion was measured on three specimens, after 15 days. After about 10 days, the specimen surface was stained with Green rust, but no crack was then visible (see Fig. 12). The first visible cracking was observed after about 20 days, its width was about 0.1 mm.
– For tests with mortar M2, in the absence of chloride a slight expansion was measured after 15 days. The specimen surfaces were then stained with white products, but no crack was visible after 24 days.

When the impressed current density is $j=500$ μA/cm^2:

– For tests with mortar M1: in the absence of chloride, no expansion was measured, after 13 days. In the presence of chlorides, an expansion was measured after 3 days and cracks filled with Green rust were visible after 4 days.
– For test with mortar M2: in the absence of chlorides, a significant expansion was measured after 10 days. Then, specimen surface was stained with white products. Large crack was observed after 17 days (Fig. 12). In the presence of chloride, an expansion was measured after 3 days and cracks filled with Green rust were observed after 4 days (Fig. 12).

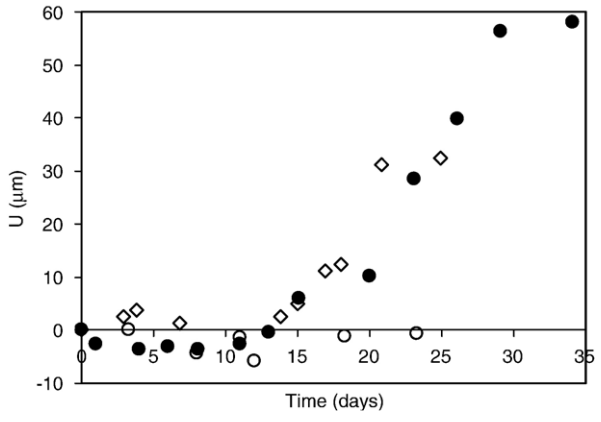

Fig. 5. Specimen expansion U (in μm) in function of time for $j=100$ μA/cm^2. With chloride: ● Mortar M1. Without chloride: ○: Mortar M1, ◇: Mortar M2.

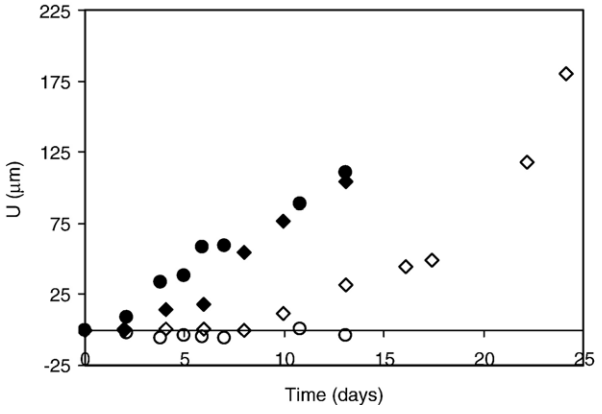

Fig. 6. Specimen expansion U (in μm) in function of time for $j=500$ μA/cm^2 with chloride: ● Mortar M1, ◆ Mortar M2, without chloride: ○: Mortar M1, ◇: Mortar M2.

Table 4
Damage of mortar

Time (days) of	Mortar M1				Mortar M2		
	j=100 μA/cm^2		j=500 μA/cm^2		j=100 μA/cm^2	j=500 μA/cm^2	
	No Cl	+Cl	No Cl	+Cl	No Cl	No Cl	+Cl
First detected expansion (day)	/	15	/	3	15	10	3
Corrosion product (day)	/	10	/	3–4	/	/	3–4
First visible crack (day)	/	20	/	4	/	<17	4

Table 4 shows the results on specimen expansion U and on its surface condition.

3.3. Electrical resistance during tests and solution conductivity

Potential drop V between counter-electrode and reinforcement was measured during the test. According to Ohm's law, the apparent specific resistance is $R=V/j$ (in Ω cm^2), where j is the current density.

The electrical specific resistance changes versus time are shown on Figs. 7 and 8 for j=100 μA/cm^2 and j=500 μA/cm^2, respectively.

For j=100 μA/cm^2, the values of the electrical specific resistance R in the two mortars were the same during the first 6 days, in every solution. Then, after 20 days, R increased in the absence of chloride, while it decreased in the presence of chloride.

For j=500 μA/cm^2, for the two mortars, the values of the electrical specific resistance were the same during the first 3 days whatever the solution. Then, after 4 days, R increased in the absence of chloride, while it decreased in the presence of chloride.

The measured specific electrical resistance R concerned both the mortar around reinforcement and the surrounding solution. So, it was of interest to separate the effects of these parameters. Fig. 9 shows the change of the solution conductivity versus time. It confirms that this conductivity is higher in chlorinated solutions than in chloride free solutions. For all tests, this conductivity first decreased with time, then it became approximately constant. The relative decrease was about 10% for chlorinated solutions, and about 50% for chloride free solutions.

So it appears that the solution conductivity change versus time is different from the global electrical specific resistance R change. This means that potential drop V and specific electrical resistance R are able to detect the formation of a reactive layer on the surface of the steel due to the impressed current and some change inside the reinforced mortar. Furthermore, it appears that

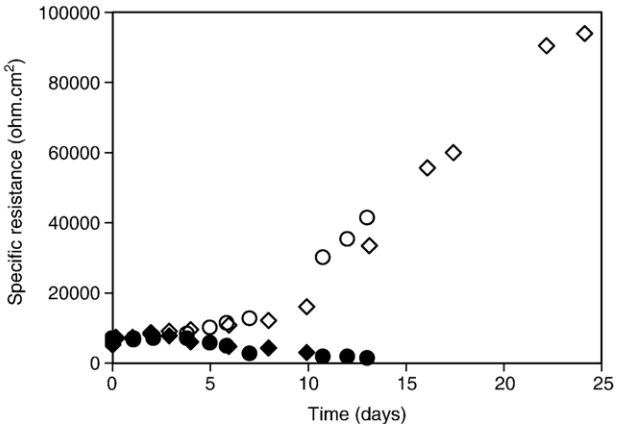

Fig. 8. Specific interfacial electrical resistance (Ω cm^2) versus time for accelerated corrosion with j=500 μA/cm^2. with chloride: ● Mortar M1, ◆ Mortar M2, without chloride: ○: Mortar M1, ◇: Mortar M2.

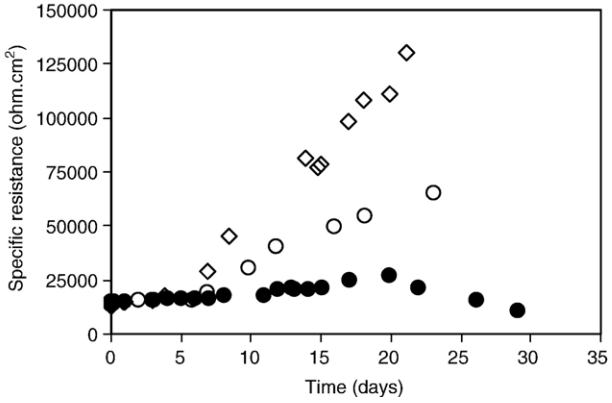

Fig. 7. Specific interfacial electrical resistance (Ω cm^2) versus time for accelerated corrosion with j=100 μA/cm^2. With chloride: ● Mortar M1. without chloride: ○: Mortar M1, ◇: Mortar M2.

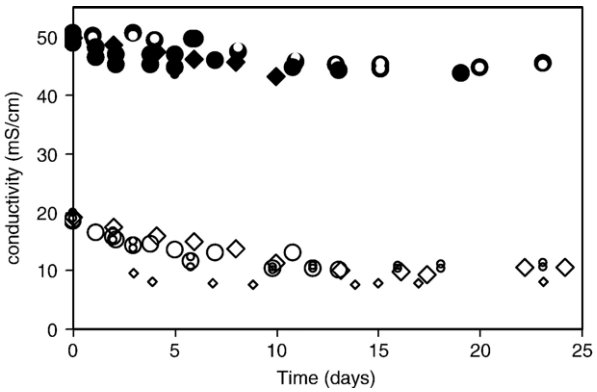

Fig. 9. Electrical conductivity of the solution versus time (in days). Diamond: mortar M1, circle: mortar M2. Open dots: chloride free solutions. Black dots: chlorinated solutions. For j=500 μA/cm^2: ◆, ●,◇, ○: Mortars M1 and M2, with and without chlorides. For j=100 μA/cm^2: ●,◇, ○: Mortars M1 and M2, with and without chlorides.

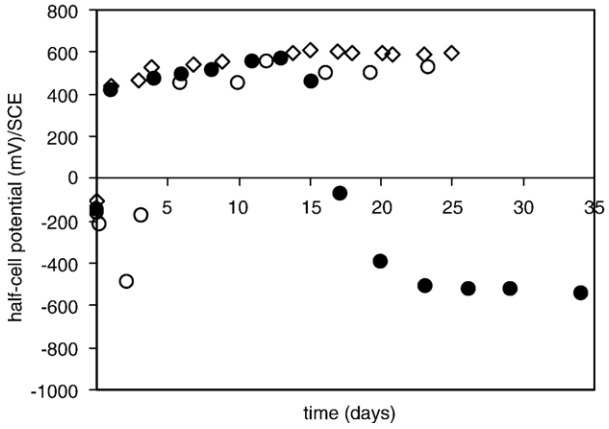

Fig. 10. Half-cell potential measured against a saturated calomel reference electrode (SCE) versus time, with $j=100$ μA/cm^2. With chloride: ● Mortar M1, without chloride: ○: Mortar M1, ◇: Mortar M2.

the electrical specific resistance R does not depend on the current density in the absence of chlorides, it increases first slightly then significantly after about one week. This means that, in this case, the change of mortar cover microstructure does not depend on the current density. In the presence of chlorides, the electrical specific resistance R increases significantly with time. This can mean that initial passivating film on steel is broken, and rust is formed.

3.4. Half-cell potential

Figs. 10 and 11 give the half-cell potential E of steel against a saturated calomel reference electrode (SCE) after current cut-off, versus time for $j=100$ μA/cm^2 and $j=500$ μA/cm^2.

The initial half-cell potential is given in Table 5 and is about -150 mV$_{SCE}$.

When the current density was $j=100$ μA/cm^2, it appears in one hand, that, for mortars M1 and M2 in chloride free solutions, half-cell potential E was first positive, it increased slightly up to about $+550$ or $+600$ mV$_{SCE}$. In the other hand, in the presence of chloride, for mortar M1, after about 15 days, half-cell potential E decreased down to -600 mV$_{SCE}$.

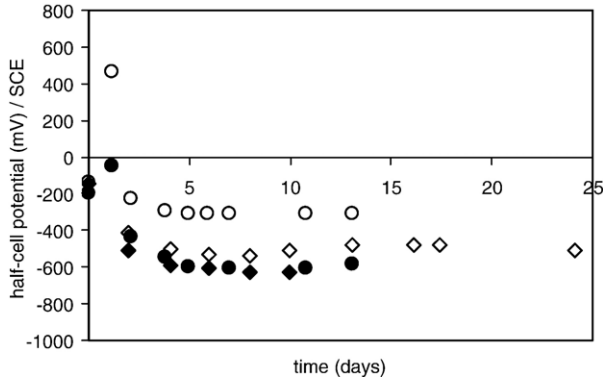

Fig. 11. Half-cell potential measured against a saturated calomel reference electrode (SCE) versus time, with $j=500$ μA/cm^2. With chloride: ● Mortar M1, ◆ Mortar M2. without chloride: ○ Mortar M1, ◇ Mortar M2.

When the current density was $j=500$ μA/cm^2, for the two mortars in every solution, half-cell potential E was first positive. Then, after about 3 days it became negative, down to -600 mV$_{SCE}$ for mortars M1 and M2, in the presence of chloride. In the absence of chloride, for mortars M1 and M2, half-cell potential E tends to -250 mV$_{SCE}$ and to -500 mV$_{SCE}$ respectively.

3.5. Characterization of corrosion pattern

At the end of each test, the reinforced mortar specimen was split off. The condition of the interface between steel and its cover was observed. It appears that:

- in the absence of chloride, for mortar M1, few brown corrosion products were observed, and in some cases, white products were observed near the steel surface. For mortar M2, black and white products were observed on steel when $j=100$ μA/cm^2. Brown rust was confined only at the interface between steel and mortar when $j=500$ μA/cm^2;
- in the presence of chloride, it appears for both mortars, that steel surface was depassivated (Fig. 12). This means that steel surface was covered with green and black products, which quickly turned red–black in contact with the atmosphere, like Green rust [12]. It appears also that corrosion products were fluid and penetrated into mortar through micro-cracks;

Fig. 13 shows optical microscope photographs of steel/mortar system cross-sections when $j=500$ μA/cm^2. SEM photographs with EDS analysis are given in Figs. 14–16 to characterize the corrosion pattern for the two mortars. Corrosion patterns are similar when $j=100$ μA/cm^2. It appears that:

- in the absence of chloride, microscopical observations show some differences between the two mortars. For mortar M1, a thin iron oxide layer is observed around steel bar. Further EDS analyses show that iron element penetrated into pores of

Table 5
Half-cell potential and corrosion products on mortar specimen surface

	Mortar M1				Mortar M2		
	$j=100$ μA/cm^2		$j=500$ μA/cm^2		$j=100$ μA/cm^2	$j=500$ μA/cm^2	
	No Cl	+Cl	No Cl	+Cl	No Cl	No Cl	+Cl
Initial half-cell potential	−165	−145	−140	−170	−100	−145	−121
Half-cell potential during accelerated test	+550	−550	−250	−600	+600	−500	−600
Product formed during test on mortar specimen surface	/	Green–Black	/	Green–Black	/	/	Green–Black

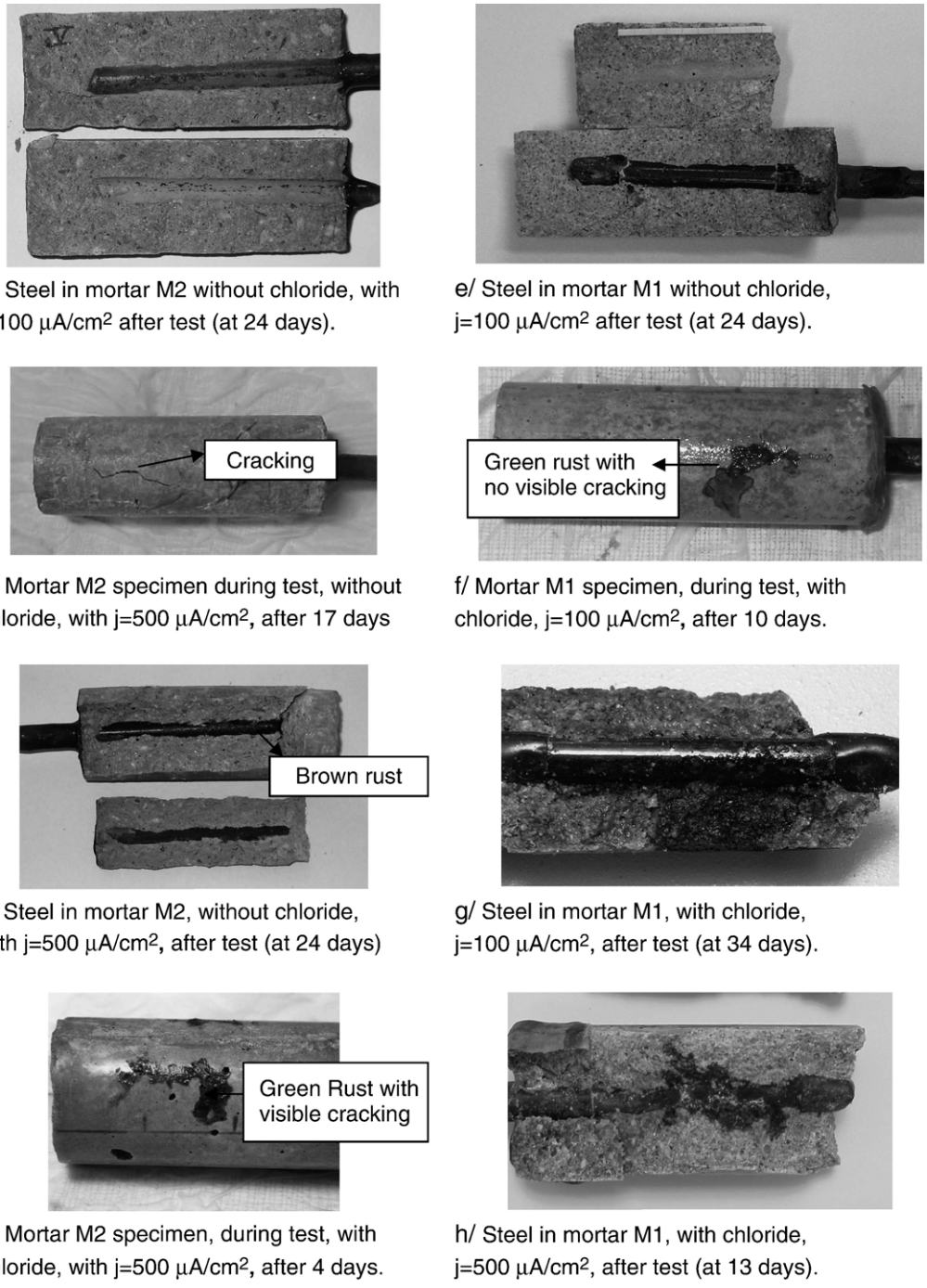

a/ Steel in mortar M2 without chloride, with j=100 μA/cm² after test (at 24 days).

e/ Steel in mortar M1 without chloride, j=100 μA/cm² after test (at 24 days).

b/ Mortar M2 specimen during test, without chloride, with j=500 μA/cm², after 17 days

f/ Mortar M1 specimen, during test, with chloride, j=100 μA/cm², after 10 days.

c/ Steel in mortar M2, without chloride, with j=500 μA/cm², after test (at 24 days)

g/ Steel in mortar M1, with chloride, j=100 μA/cm², after test (at 34 days).

d/ Mortar M2 specimen, during test, with chloride, with j=500 μA/cm², after 4 days.

h/ Steel in mortar M1, with chloride, j=500 μA/cm², after test (at 13 days).

Fig. 12. Steel and mortar specimens during and after accelerated corrosion test, with $j=100$ μA/cm^2 and with $j=500$ μA/cm^2.

mortar (Fig. 17). For mortar M2, rather thick corrosion (about 300 μm) products are observed around steel bar. These differences may be explained by the fact that mortar M1 is more porous, so iron can migrate into its pores. A further analysis, by using EDS, showed that the white products which are observed near the steel interface and on the specimen surface include calcium (Fig. 17). These products can result from the migration of Ca^{+} under the electrical field.

– in the presence of chloride, for the two mortars, homogeneous corrosion products and pitting are observed with optical microscope. It is to be noticed that a macroscopic crack in mortar was observed at the vicinity of the steel/mortar interface and localized iron dissolution and corrosion products were observed (Fig. 13). The X-ray cartography using the distribution of O, Ca, Si and Fe elements, shows that iron (Fe) and mortar (Ca, Si) are well-identified. Chlorine is identified in mortar. Furthermore, the interface area is rich of Fe and O elements which confirms the presence of iron oxides or hydroxides. Calcium element is sometimes observed in the rust layer. A very little amount of iron element is observed in the mortar. Thus, the following

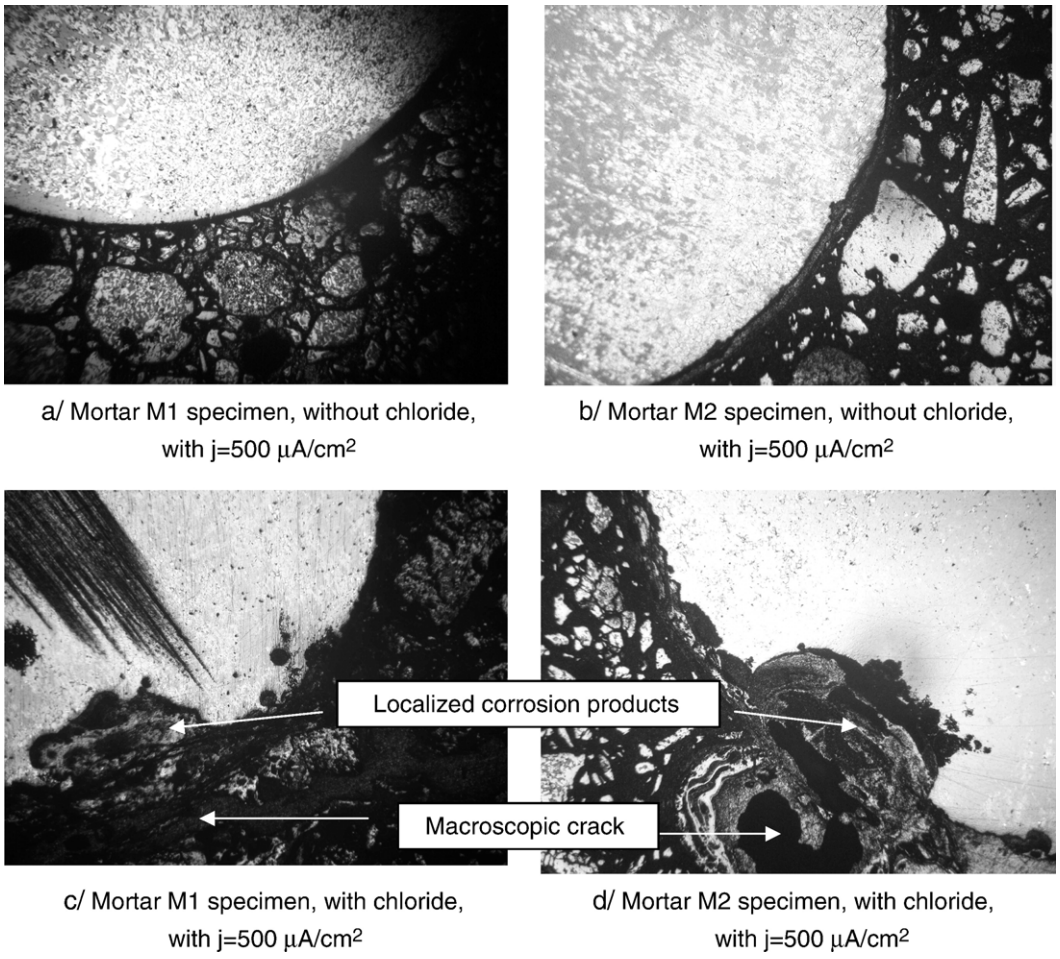

Fig. 13. Optical microscope (OM) photographs of steel/mortar interface (steel diameter is 8 mm).

corrosion pattern is characterized by: metallic substrate, product layer and binder. Furthermore, far from the macroscopic crack, the rust layer is homogeneous, but irregular, around rebar. The thickness of the product layer is about 150–200 μm for mortar M2 and 100–150 μm for mortar M1. This result agrees with the fact that iron migrates more easily in the coarser porosity of mortar M1. For the mortar M2 with chlorides, the trace of the original rebar diameter can be seen (see D/ in Fig. 14). This shows that, far from the macroscopic crack, the rebar section reduction is about 50–60 μm.

3.6. Concluding remarks

These results show that in chlorinated solutions the effect of the impressed current is the same for mortars M1 and M2 whatever the current density. Steel is depassivated in chlorinated solutions whatever the current density and the type of mortar. For all these cases, Green rust was observed at the steel–mortar interface and the mortar cover was cracked. Corrosion products are confined between steel and mortar.

In the absence of chloride, in any mortar, steel is depassivated whatever the current density. Then, brown rust was observed at the mortar surface and at its interface with the embedded steel. Swelling and cracking were observed with mortar M2, but no expansion was detected for mortar M1. The values of half-cell potential agree with corrosion conditions, when $j = 500\ \mu A/cm^2$.

4. Discussion

4.1. General effect of impressed current

When steel embedded in mortar is anodically polarized by means of a counter-electrode, various anions in mortar, e.g. chloride, will migrate to the steel surface, and simultaneously cations, (iron, etc.) will migrate to the outer surface of the mortar specimen. These migrations of ions in mortar can change the microstructure and some properties of the cover, as these will also occur for cathodic polarization [13]. For example, it appears that under accelerated tests, calcium can flow out of mortar to its surface.

So, it is important to check if the corrosion process is the same under natural corrosion and in impressed current technique. Numerous models are proposed in literature to estimate the time for first cracking, t_c, induced by corrosion products. For example in [14], t_c in reinforced concrete is proportional to the reverse of current density, when it is assumed that the mass of reacting steel during the corrosion

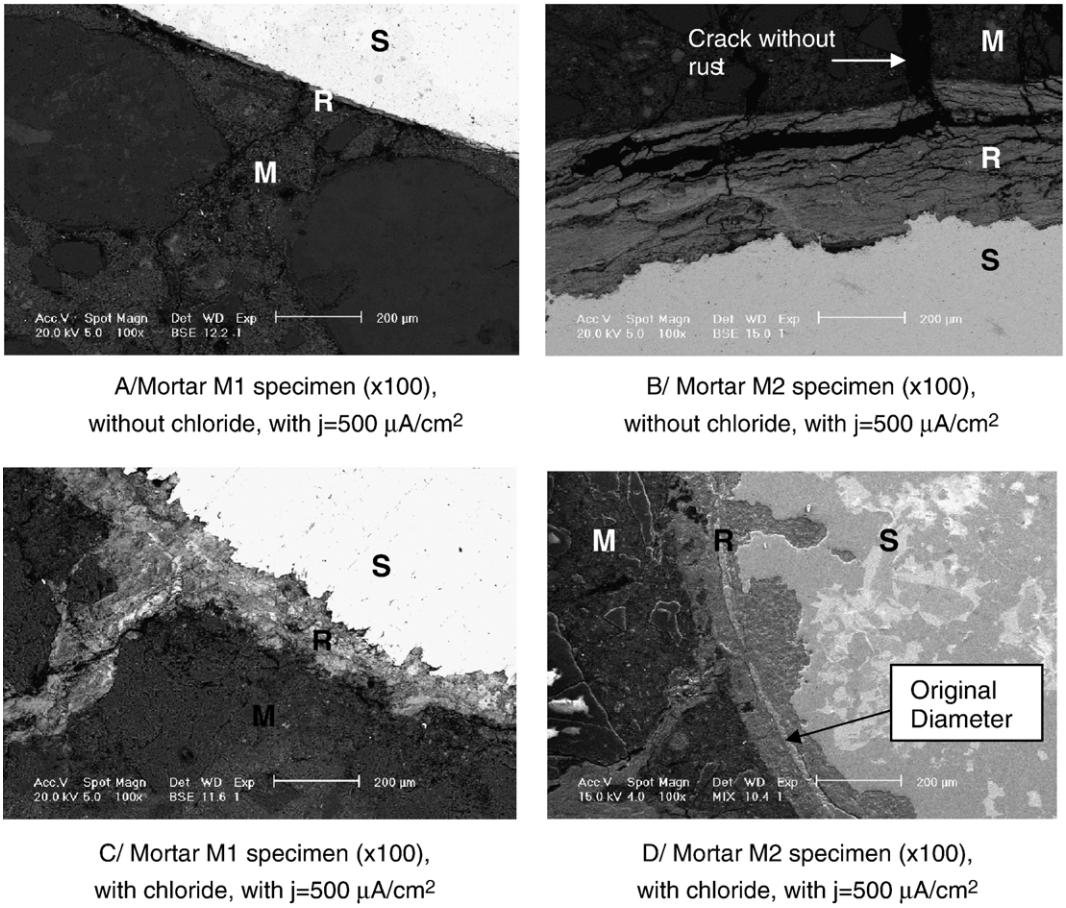

Fig. 14. Scanning electron microscope (SEM) photographs of steel/concrete interface with S (steel), R (rust layer), M (mortar).

process obeys Faraday's equation and that corrosion products are around steel rebar. But the transference number, is not well known for an accelerated corrosion test. This means that the amount and moving rate of each migrating ion are unknown. In addition, iron dissolution is not the only reaction, which takes place at the anode, other reactions can also occur, e.g. water oxidation [15]. So, Faraday's law is questionable, and it is of importance to check if iron dissolution is the main process involved in accelerated corrosion tests. This point will be discussed after summarizing the main results obtained.

4.2. Accelerated corrosion of steel in mortar with chlorinated solutions

The natural corrosion of steel in concrete includes several stages. Ideally, the results of accelerated tests should comply with this process. Critical times related to corrosion stages, are determined using mortar expansion and full cracking, steel half-cell potential, as well as potential drop (electrical resistance) between cathode and rebar.

4.2.1. Expansion curve

A critical time can be related to a critical expansion $U=5$ μm, the corresponding tensile strain at steel–mortar interface is then about 3.10^{-4}. This critical value of the strain is higher than the ultimate strain of mortar under tension. This means that at this level micro-cracks will have formed at the interface between steel and mortar.

The results show that in the presence of chlorides, this critical value is measured after 15 days for $j=100$ μA/cm^2 (mortar M1) and after about 3 days for $j=500$ μA/cm^2 (mortars M1, M2).

It should be noted that mortar expansion starts only after mortars' pores close to steel are completely filled with corrosion products, which induce mortar cover expansion [16].

4.2.2. Visible cracking

Another critical time corresponds to the occurrence of the first visible crack (about 0.1 mm wide). The first visible crack in the presence of chlorides was observed after 4 days when $j=500$ μAc/m^2 and after 20 days when $j=100$ μA/cm^2.

4.2.3. Half-cell potential

Another critical time can be defined when the half-cell potential (measured against a saturated calomel electrode) becomes negative. Then, for $j=100$ μA/cm^2 and for mortar M1, a first critical time (about 15 days) is defined when the half-cell potential begins to decrease and a second critical time (about 20 days) is defined when the half-cell potential has attained a

stable negative value. For $j=500$ μA/cm^2 these critical times are about 3 days and 4 days for mortars M1 and M2, respectively.

The meaning of these critical times is not very precise, as the half-cell potential value depends on the condition of the embedded steel, on oxygen content [17], on chloride content

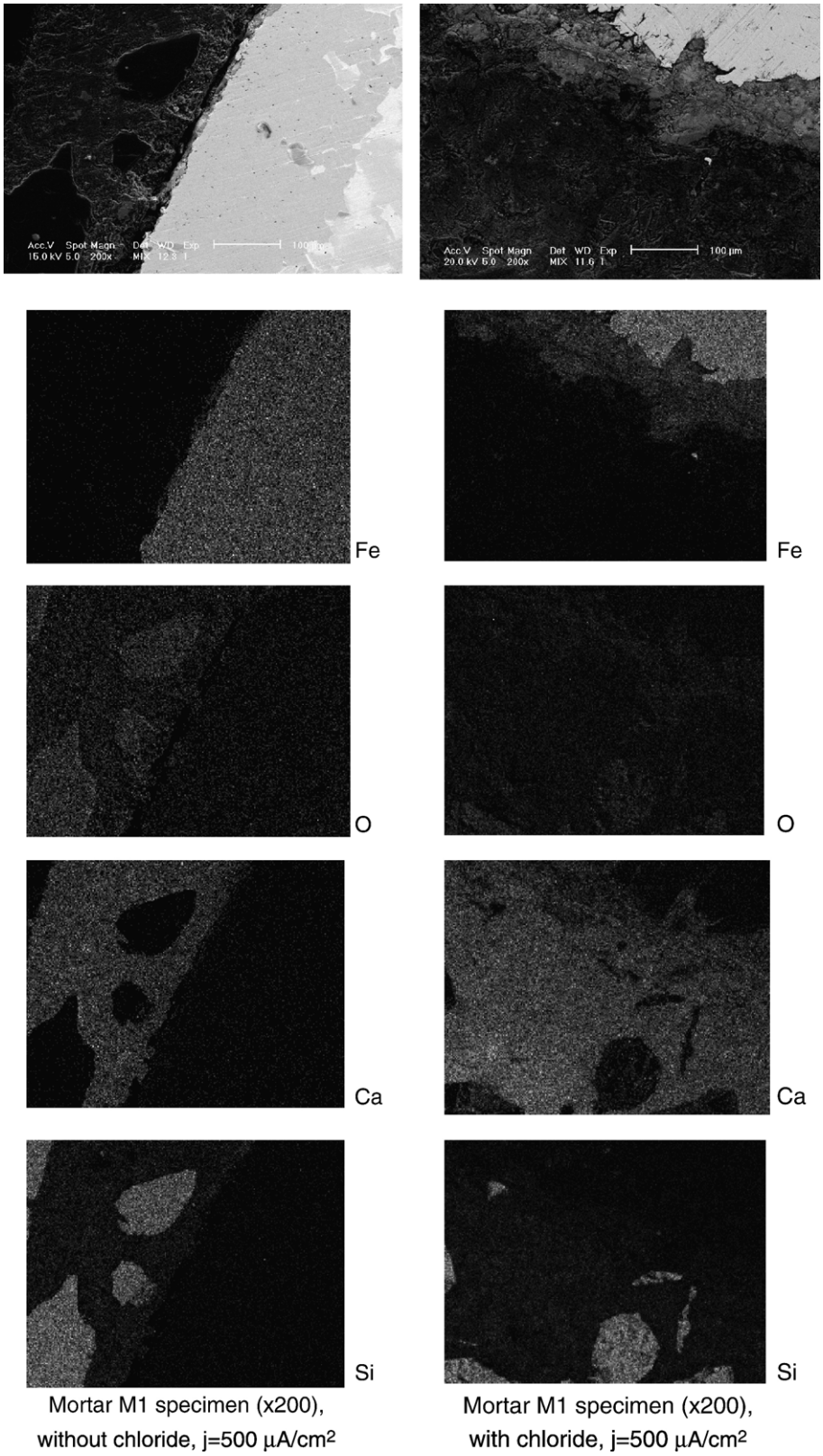

Fig. 15. Elements distribution of steel/mortar interface for specimen M1, Fe (iron), O (oxygen), Ca (calcium), Si (silicon).

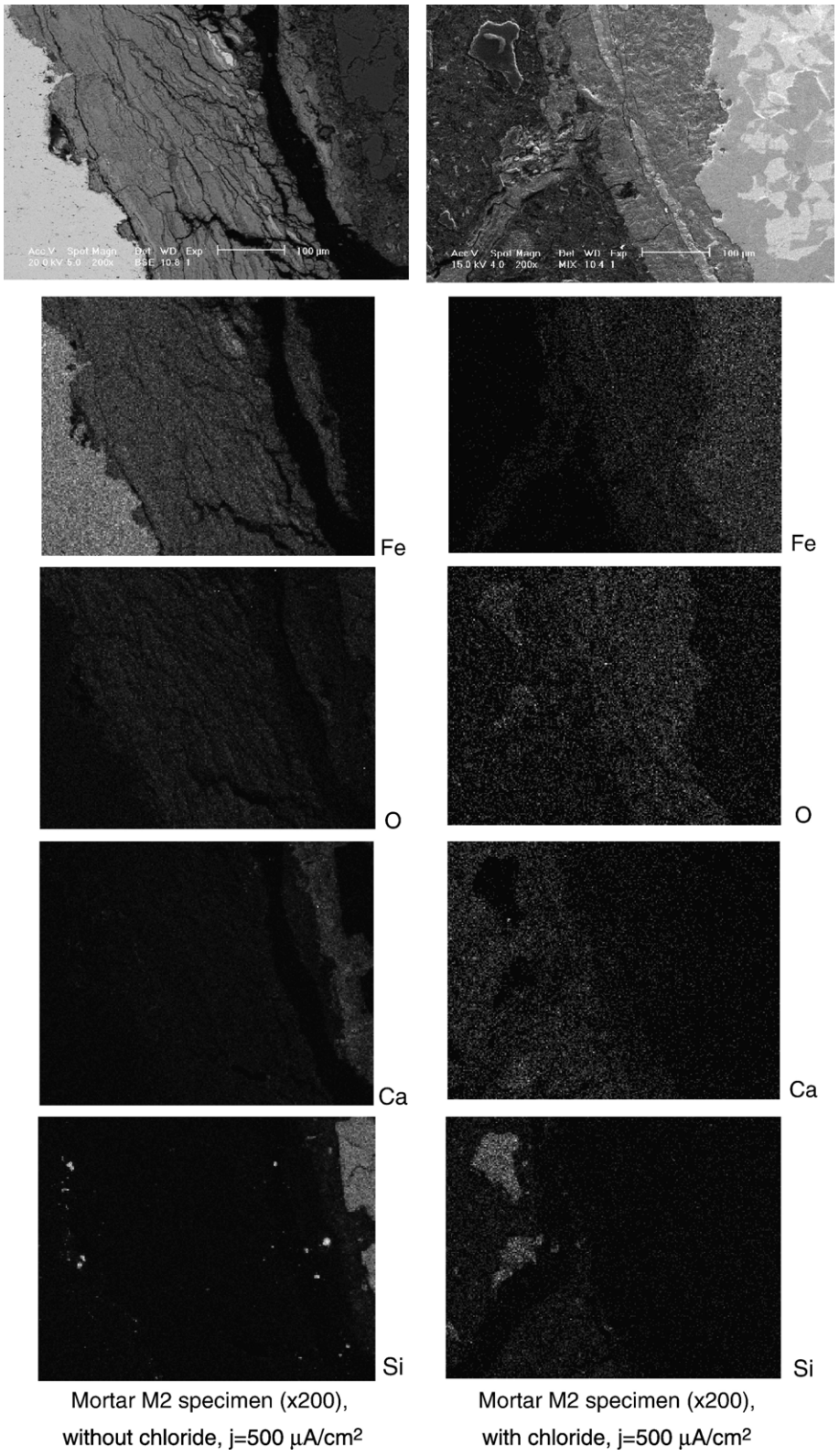

Fig. 16. Elements distribution of steel/mortar interface for specimen M2, Fe (ion), O (oxygen), Ca (calcium), Si (silicon).

[18], on cover cracking and type of iron oxides [19]. So, the critical times based on half-cell potential are to be compared with the other critical times defined by the expansion curve and the appearance of the microcracking between steel and mortar. The decrease of half-cell potential is likely due to a lack of oxygen at the interface between steel and mortar. This occurs when compact oxides are formed on the steel surface [19]. This result agrees with the presence of fluid corrosion products and

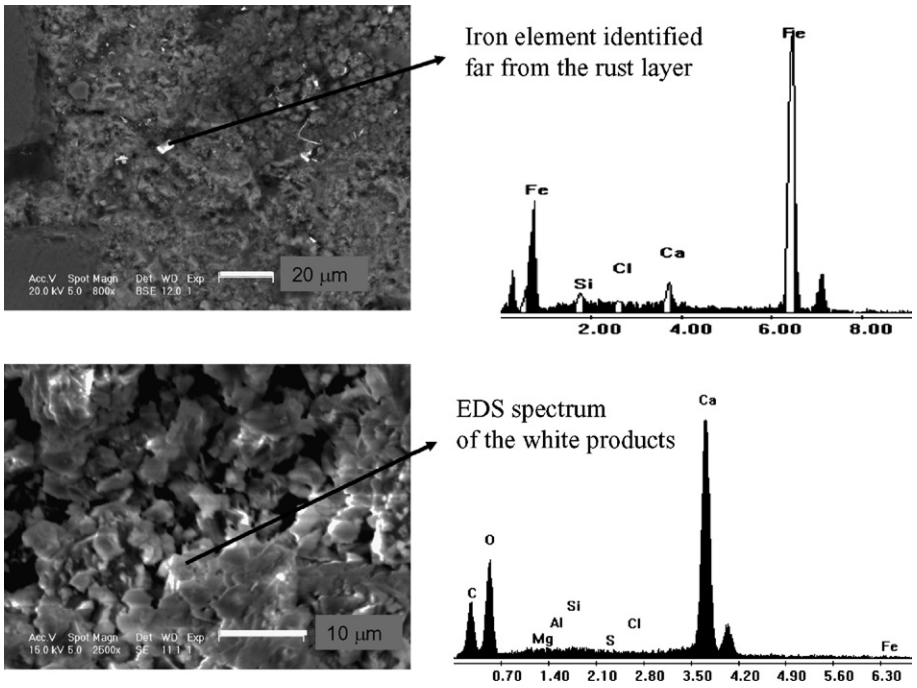

Fig. 17. Characterization of iron element far from the steel/mortar interface and of white products by SEM and surface analysis (EDS).

with mortar expansion and microcracking. Furthermore, in the case of specimens in chloride free solution, rust is not fluid, and the value of the half-cell potential is the same before and after expansion or cracking (M2, $j=500$ μA/cm^2) as for [19].

4.2.4. Electrical resistance (potential drop)

An alternative definition of critical time is related to the potential drop V between rebar and counter-electrode, or specific electrical resistance $R=V/j$, where j is the current density. A critical time corresponds to a steep decrease of V or R in a short period of time. So, in the presence of chlorides, for $j=100$ μA/cm^2, the specific resistance R slowly increases, and after about 20 days, it decreases. In the presence of chlorides, for $j=500$ μA/cm^2, the specific resistance R slowly decreases and a critical time is observed at about 4 days.

Then, as potential drop V and electrical specific resistance R are related to a formation of products on steel surface, they may be indicators of corrosion initiation, even when a direct current is applied. The decrease of the resistance of the reactive layer on the surface of the steel has been attributed to the corrosion initiation period by [20]. But in this study, specific resistance characterizes also some mortar properties because during the accelerated test, ions migrate through mortar under the influence of an electrical field. As mentioned in [21,22] in a study on accelerated tests, migrating ions are accumulated in pore solutions and change the electrical resistance of concrete, which may first decrease, then increase with time.

So, the increase of specific resistance results from some changes of the layer at the steel–mortar interface and of the mortar composition. The decrease of the specific resistance is due to the presence of a crack. Similar results have been obtained by [7] during accelerated corrosion tests too. When the mortar cover is cracked, the surrounding solution fills this crack and results in a decrease of the potential drop between the steel and the counter-electrode.

4.2.5. Concluding remarks

Table 6 gives critical times related to the potential drop for mortars M1 and M2. No difference is observed between these two mortars placed in chlorinated solution. For $j=100$ μA/cm^2 the critical time is 20 days and for $j=500$ μA/cm^2, this time is 4 days. The process of reinforcement mortar due to impressed current with chlorinated solutions is done in Fig. 18. The definitions of the critical times used in this study are quite different from those proposed by [2,3]. Here critical times characterize mortar cover expansion due to corrosion products on steel, starting from corrosion initiation up to visible cracking. But the real first depassivation time cannot be determined from potential drop and half-cell potential measurements.

4.3. Corrosion products and corrosion pattern

Another objective of this study is to check whether products formed under accelerated corrosion tests are the same as the ones, which are formed under natural exposure conditions.

Table 6
Critical times of steel corrosion in mortar due to impressed current for the two mortars M1 and M2 for the tests with chlorinated solution

Critical time t_c (days) determined by	$j=100$ μA/cm^2	$j=500$ μA/cm^2
	t_c	t_c
Expansion curve	15	3
Cracking	20	4
Half-cell potential	15/20	3/4
Electrical resistance	20	4

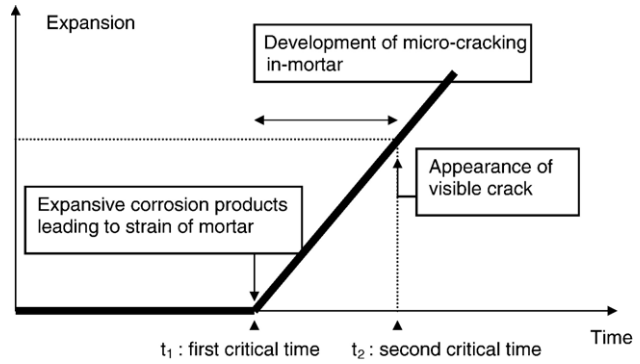

Fig. 18. Expansion versus time. Schematic process of reinforcement corrosion in mortar exposed to chlorinated solutions due to impressed current.

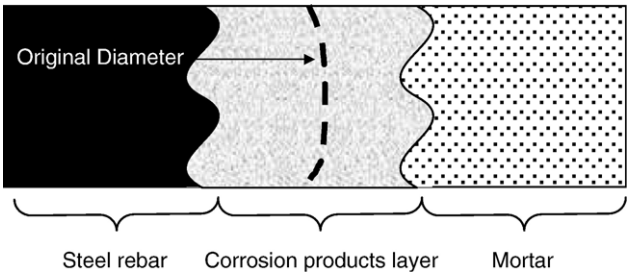

Fig. 19. Schematic description of the corrosion layer structure in mortar exposed to chlorinated solutions due to impressed current.

Table 7 gives the type of products obtained after this study. Indeed, all iron oxides have vivid colors, which can also be used for their characterization [23].

In a natural chloride free environment, steel embedded in concrete does not corrode. So, for an impressed current, in a chloride free solution, corrosion does not correspond to real conditions.

In a chlorinated natural environment, steel corrosion in concrete results from a depassivation due to chlorides. This means that the passivation products are transformed in non-protective products through two main stages. In a first step, transient products, called Green rust, are formed [12,24]. Then, in the absence of oxygen they can become magnetite. But in most cases, oxygen is present and these products become FeOOH (lepidocrocite, akageneite, etc.). This process agrees with some results, which show that corrosion products of iron in chlorinated environment include Fe^{2+} and Fe^{3+} [25–27].

In this study, Green rust was observed for a couple of minutes, then turned into ordinary red rust. The reddish corrosion products are ordinary rust (lepidocrocite or possibly akageneite). Only a few data are available for accelerated corrosion of steel embedded in concrete immersed in chlorinated solutions. For example, akageneite is the main product formed under accelerated conditions, on steel in concrete immersed in NaCl solution [30]. Another study [31] reports that akageneite, magnetite, goethite are formed on steel cast in concrete containing chloride, under a constant voltage to accelerate corrosion. The same products were identified by XRD analysis after accelerated corrosion tests carried out with mortar M2 containing chlorides [10]. So, the types of corrosion products which are formed for accelerated corrosion test are the same as for natural corrosion.

Furthermore, the corrosion patterns in these two cases are similar with what is obtained under natural corrosion. Fig. 19 shows the corrosion layer structure in the presence of chloride. This structure agrees with the natural corrosion pattern [28,29]. In some cases, corrosion products penetrate into cement pores. Nevertheless, calcium element is sometimes observed in the corrosion layer formed during accelerated tests. This is possibly due to an acidification of the solution near the steel rebar inducing the dissolution of portlandite. This acidification can induce an additional corrosion as mentioned by [33].

4.4. Effect of the current density

If the only effect of an impressed current is to accelerate the dissolution rate of iron, the amount of dissolved metal depends only on the total amount of electrical charge passed, according to Faraday's law.

In Fig. 20, the specimen expansion U is plotted against the total amount of electrical charge passed. It appears that:

- in solutions free of chlorides, there is no general relationship between expansion U and electrical charge.
- in chlorinated solution, expansion U at a given time does not depend on the mortar (M1 and M2) and there is a relationship between expansion U and electrical charge. This difference may be attributed to chlorides, which modify the corrosion mechanisms [26]. Furthermore the level of current density has no effect on the damage development in mortar: the critical times for $j=100$ μA/cm^2 are about five times less than that for $j=500$ μA/cm^2. For all cases, mortar cover begins to expand when the reinforcement radius loss

Table 7
Half-cell potential and corrosion products on rebar surface according [23]

	Mortar M1				Mortar M2		
	$j=100$ μA/cm^2		$j=500$ μA/cm^2		$j=100$ μA/cm^2	$j=500$ μA/cm^2	
	No Cl	+Cl	No Cl	+Cl	No Cl	No Cl	+Cl
Half-cell potential during accelerated test	+550	−550	−250	−600	+600	−500	−600
Products on rebar surface	Brown	Green–Black	Brown	Green–Black	Black	Brown	Green–Black
Iron oxides	Goethite	Green Rust* +Magnetite	Goethite	Green Rust* +Magnetite	Magnetite	Goethite	Green Rust* +Magnetite

(*: Green rust, which turned reddish ordinary rust).

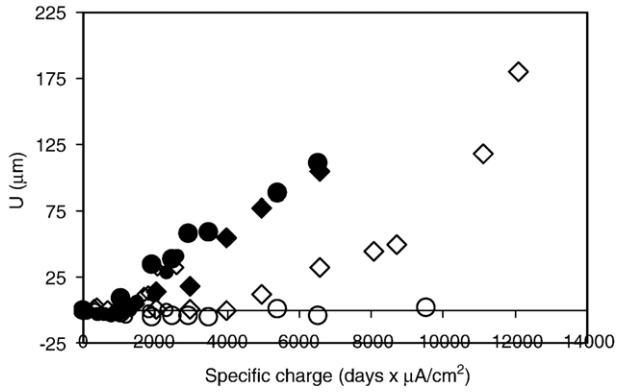

Fig. 20. Specimen expansion U (µm) in function of specific total electrical charge=time×current density (days×µA/cm^2). Diamond: mortar M1, circle: mortar M2, Open dots: chloride free solutions Black dots: chlorinated solutions for j=100 µA/cm^2: ●,◇,○: Mortars M1 and M2, with and without chlorides. for j=500 µA/cm^2: ◆,●,◇,○: Mortars M1 and M2, with and without chlorides.

calculated from Faraday's law is about 47 µm and visible cracking corresponds at radius loss of about 63 µm whatever the current density. The value of this critical radius loss obtained agrees with data published by other authors [33] for accelerated corrosion tests using impressed current.

To verify whether iron dissolution is the main anodic process involved, some authors used parameter N (current efficiency), which represents the ratio between the charge needed for oxidizing iron and the total charge passed. The current efficiency value is obtained by comparing the real gravimetical mass loss and the theoretical value given by Faraday's law [9,32,33]. In [32], N is about 70% for a current density equal to 400 µA/cm^2. According to [9], N=100% for various current densities (j=100, 200, 350, 500 µA/cm^2). But published results often indicated current efficiencies higher than 100% [33]. So, the experimental conditions of accelerated tests have possibly an influence on the process involved.

In this study, the weight losses of rebars were not determined, but the rebar section loss far from the macroscopic crack was compared to its theoretical value obtained by Faraday's law. For the mortar M2 with chlorides, after 4 days of tests, the section reduction is equal to 63 µm. The experimental measurements give 50–60 µm far from the macroscopic crack. So, in this case, iron dissolution is the main processes during accelerated tests and that steel corrosion obeys Faraday's law during accelerated tests. This result agrees with the fact that the corrosion process is more active near the macroscopic crack, which is visible after 4 days. Although additional processes can occur (water oxidation, iron migration into cement pores) it appears that Faraday's law may be used to determine the times to cracking, as shown in Figs. 18 and 20.

5. Conclusions

The object of this study is to check how accelerated corrosion tests simulate steel corrosion in real reinforced concrete structures. In these tests, corrosion is accelerated, by polarizing reinforcement against a counter-electrode, with an anodic current. The real structures are usually exposed to atmosphere, and this is to be compared with the accelerated tests, which are carried on reinforced mortar specimens, immersed in aqueous solutions with or without chloride.

The results obtained show that, like under natural condition, in accelerated tests, rust formed on steel expands, makes its concrete cover crack, and induces a loss of bonding between reinforcement and concrete. The corrosion products obtained are similar to what is observed under natural condition. In accelerated tests, the time when cracking starts, can be detected by using two methods. The first method deals with measuring the potential drop between counter-electrode and reinforcement, while the current is maintained constant. The second method deals with measuring specimen expansion versus time. These two methods give the same results and show that accelerated tests make it possible to detect the first cracking and the beginning of bonding loss.

In real reinforced concrete structures, steel corrosion is due either to concrete carbonation or to concrete pollution by chloride. In the accelerated tests applied, specimens are immersed in solutions containing or not chloride. The results obtained with these accelerated tests show that steel corrosion obeys Faraday's law, only when specimens are in chlorinated solution. This means that the main process involved is then steel dissolution. On the contrary, when pure water is used, a more complex process occurs during accelerated corrosion test, even for current density not higher than 500 µA/cm^2. Some complementary studies show that the properties of mortar around steel are changed.

So, accelerated corrosion test by impressed current is confirmed to be a valid method to study the corrosion process of steel in concrete, and its effects on the damage of concrete cover. This study shows also that cracks appearance and propagation in concrete can be monitored with non destructive techniques.

References

[1] J.A. Gonzales, S. Feliu, P. Rodriguez, E. Ramirez, C. Alonso, S. Andrade, Some questions on the corrosion of steel in concrete — Part I: when, how and how much steel corrodes, Materials and Structures 29 (January–February 1996) 40–46.
[2] K. Tuutti, Corrosion of steel in concrete, CBI research report no 4.82, Swedish Cement and Concrete Research Institute, Stockholm, Sweden, 1982.
[3] P.D. Cady, R.E. Weyers, Chloride penetration and the deterioration of concrete bridge decks, Cement, Concrete and Aggregates 5 (2) (1983) 81–87.
[4] R. Francois, G. Arliguie, Effect of microcracking and cracking on the development of corrosion in reinforced concrete members, Magazine of Concrete Research 51 (2) (1999) 143–150.
[5] H. Hidrissi, A. Liman, Study and characterization by acoustic emission and electrochemical measurements of concrete deterioration caused reinforcement steel corrosion, NDT&E International 36 (2003) 563–569.
[6] J.G. Cabrera, Deterioration of concrete due to reinforcement steel corrosion, Cement and Concrete Composites 18 (1996) 47–59.
[7] C. Fang, K. Lundgren, L. Cheng, C. Zhu, Corrosion influence in reinforced concrete, Cement and Concrete Research 34 (2004) 2159–2167.
[8] C. Andrade, C. Alonso, F.J. Molina, Cover cracking as a function of bar corrosion: Part I — experimental test, Materials and Structure 26 (1998) 453–464.

[9] T.A. El Maaddawy, K.A. Soudki, Effectiveness of impressed current technique to simulate corrosion of steel reinforcement in concrete, Journal of Materials in Civil Engineering (January/February 2003) 41–47.
[10] Q.T. Nguyen, Etude expérimentale et théorique de l'effet de la corrosion sur la fissuration du béton et sur le comportement global des structures en béton armé. Ph.D, Université Paris VI, 2006, (in french).
[11] S. Caré, Aggregate influence on chloride ion diffusion into mortar, Cement and Concrete Research 33 (2003) 1021–1028.
[12] J.M.R. Genin, Ph. Refait, A. Raharinaivo, Green rusts, intermediate corrosion products formed on rebar in concrete in the presence of carbonation or chloride ingress, International Conference Understanding Corrosion Mechanisms of Metals in Concrete: A Key to Improving Infrastructure Durability, July 27–31 1997, Cambridge, USA.
[13] T.D. Marcotte, C.M. Hansson, B.B. Hope, The effect of the electrochemical chloride extraction treatment on steel-reinforced mortar. Part II: microstructural characterization, Cement and Concrete Research 29 (1999) 1561–1568.
[14] R. Piltner, P.J.M. Monteiro, Stress analysis of expansive reactions in concrete, Cement and Concrete Research 30 (2000) 843–848.
[15] A.A. Hachemi, M. Murat, J.C. Cubaud, Recherche sur l'accélération de la corrosion des aciers dans le béton — Etude électrochimique théorique et expérimentale, Revista Materiales Para La ConstruccioÂn 700 (3) (1976) 149–155.
[16] Y. Liu, R.E. Weyers, Modeling the time-to-corrosion cracking in chloride contaminated reinforced concrete structure, ACI Material Journal, Technical paper, 1998.
[17] J.A. Gonzales, E. Otero, S. Feliu, W. Lopez, Initial steps of corrosion in the steel/$Ca(OH)_2+Cl^-$ system: the role of heterogeneities on the steel surface and oxygen supply, Cement and Concrete Research 23 (1993) 33–40.
[18] B.H. Oh, S.Y. Yang an, Y.S. Shin, Experimental investigation of the threshold chloride concentration for corrosion initiation in reinforced concrete structures, Magazine of Concrete Research 55 (2) (2003) 117–124.
[19] A. Ouglova, A. Raharinaivo, Y. Berthaud, I. Petre-Lazar, H. Boukhenhouf, Numerical simulation of potential distribution to the corrosion of reinforcement in concrete structures, Materials and Structures 38 (281) (2005) 711–719.
[20] O. Poupard, A. Ait-Mokhtar, P. Dumargue, Corrosion by chlorides in reinforced concrete: determination of chloride concentration threshold by impedance spectroscopy, Cement and Concrete Research 34 (2004) 991–1000.
[21] W. Prince, J.P. Ollivier, O. Truc, Aspects électrochimiques de l'essai accéléré de perméabilité aux ions chlorures, Materials and Structures 32 (1999) 243–251.
[22] W. Prince, R. Pérami, M. Espagne, Mechanisms involved in the accelerated test of chloride permeability, Cement and Concrete Research 29 (1999) 687–694.
[23] U. Schwertmann, R.M. Cornell, Iron Oxides in the Laboratory, Preparation and Characterization, VCH, 1991.
[24] J.M.R. Genin, A. Raharinaivo, B. Kounde, A.A. Olowe, D. Rezel, Ph. Bauer, The corrosion products of suspension cables and concrete rebars, studied by Mössbauer spectroscopy, 11th International Corrosion Congress, Florence (I.), vol. 1, April 1990, pp. 1591–1598.
[25] K.K. Sagoe-crentsil, F.P. Glasser, Steel in concrete: Part I. A review of the electrochemical and thermodynamic aspects, Magazine of Concrete Research 41 (149) (1989) 205–212.
[26] K.K. Sagoe-Crentsil, F.P. Glasser, "Green rust", iron solubility and the role of chloride in the corrosion of steel at high pH, Cement and Concrete Research 23 (1993) 785–791.
[27] M. Pourbaix, Thermodynamics and corrosion, Corrosion Science 30 (10) (1990) 963–988.
[28] O. Poupard, V. L'Hostis, S. Catinaud, I. Petre-Lazar, Corrosion damage diagnosis of a reinforced concrete beam after 40 years natural exposure in marine environment, Cement and Concrete Research 36 (3) (2006) 504–520.
[29] W.J. Chitty, P. Dillmann, V. L'Hostis, C. Lombard, Long-term corrosion resistance of metallic reinforcements in concrete—a study of corrosion mechanisms based on archeaeological artifacts, Corrosion Science 47 (2005) 1555–1581.
[30] M. Murat, M. Charbonnier, A. Ahmadi Hachemi, J.C. Cubaud, Nature particulière des oxydes de fer hydratés formés dans certaines conditions de corrosion accélérée de l'acier dans le béton, Cement and Concrete Research 4 (1974) 945–952.
[31] I. Petré-Lazar, Evaluation du comportement en service des ouvrages en béton armé soumis à la corrosion des aciers, outil d'aide à la décision, Ph.D, Université Laval, Québec, 2000, in french.
[32] Y. Ballim, J.C. Reid, Reinforcement corrosion and the deflection of RC beams — an experimental critique of current test methods, Cement and Concrete Composites 25 (2003) 625–632.
[33] C. Alonso, C. Andrade, J. Rodriguez, J.M. Diez, Factors controlling cracking of concrete affected by reinforcement corrosion, Materials and Structures 31 (1998) 435–441.